Numerical Modeling of Axisymmetric Coaxial Waveguide Discontinuities

Gregory M. Wilkins, *Student Member, IEEE*, Jin-Fa Lee, *Member, IEEE*, and Raj Mittra, *Fellow, IEEE*

Abstract—**Techniques for determining field behavior in the presence of coaxial-to-coaxial discontinuities are presented for axisymmetric geometries. A bilinear functional is formulated from which field solutions are obtained by way of the finite element method. An absorbing boundary condition is applied at the input and output port boundaries to reduce the size and complexity of the problem. An additional approach, mode matching, is outlined and presented as verification of finite element results. Two geometries are investigated, for which numerical results are presented. A comparative evaluation of the two techniques is included.**

I. Introduction

ELECTROMAGNETIC energy is frequently transported within an electrical network by way of coaxial transmission lines. However, the dimensions of the individual components included in the network tend to vary. These differences in dimension are most prevalent at the interfaces between the respective regions containing the components. The focus of our investigation is the field behavior in the presence of these coaxial-to-coaxial interfaces. Specifically, we are interested in junctions which occur between a system of cascaded coaxial lines as encountered, for example, in high-frequency connectors [1]. At such junctions problems such as dispersion, loss, non-fundamental-mode propagation, and impedance discontinuities are commonplace and thus warrant special attention.

The waveguide junction problem has previously been investigated with an emphasis on rectangular geometries [2]–[5]. The use of Cartesian coordinates is satisfactory in these instances. However, since the task of designing high-speed digital circuits is quite involved, any method of simplifying the analysis is beneficial. It is therefore to our advantage to make use of an alternative, more suitable coordinate system and to adapt it to our problem, as suggested by Konrad [6], Daly [7], and Gwarek [8]. Hence, the numerical techniques employed in this research are formulated in terms of cylindrical coordinates. These techniques enable us to analyze many configurations repeatedly and consistently without major modifications to the approaches. We are also able to predict the field distribution throughout all regions and the corresponding energy reflection and transmission at the interfaces, from which we may develop an equivalent circuit model for the transmission line network. This information may be used to optimize the design procedure.

Manuscript received November 21, 1990; revised March 29, 1991.

The authors are with the Department of Electrical and Computer Engineering, University of Illinois, Urbana IL 61801.

IEEE Log Number 9101009.

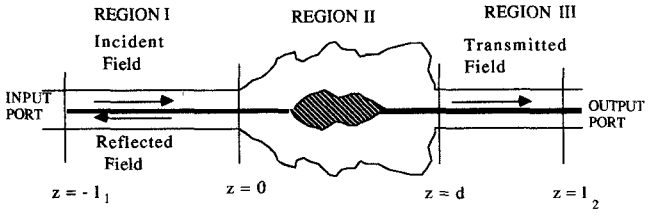

Fig. 1. General three-region axisymmetric coaxial configuration.

One approach, the finite element method (FEM) [9], provides a means of characterizing high-frequency connectors without tedious trial and error experimentation. It is also very general in that it enables us to solve problems with irregular geometries that cannot be conveniently handled using conventional approaches. Another technique, mode matching [10]–[12], serves as an excellent means of verifying the results obtained through use of the FEM.

II. Numerical Modeling

The geometries of interest are axisymmetric; i.e., they have no variation in the azimuthal direction. We may, therefore, focus our attention on one azimuthal plane of the problem. Fig. 1 shows a general three-region axisymmetric coaxial configuration. We see that we may also exploit the radial symmetry and model only the upper half of the cross-sectional area shown. Region I contains both the incident and reflected fields, and is referred to as the input port. In a similar fashion region III contains the transmitted field and is hence the output port. Region II is the region of the discontinuity and has field activity in both the positive and negative directions. Currently our interest is directed toward situations where regions I and III are homogeneous and only the fundamental propagation mode exists at the input and output ports. This corresponds to transverse electromagnetic (TEM) mode propagation.

There may exist, however, non-TEM-mode field activity in the region of the discontinuity, region II. Owing to the azimuthal symmetry of the problem, the non-TEM modes in region II will be strictly transverse magnetic. The

0018-9480/91/0800-1323$01.00 ©1991 IEEE

associated field components are H_ϕ and E_ρ in regions I and III, with E_z also being present in region II. We begin our investigation by first formulating the problem in terms of a finite element approach and following up with an overview of the mode-matching technique.

III. Finite Element Method

Beginning with Maxwell's equations,

$$\vec{\nabla}\times\vec{H}=j\omega\epsilon(\rho,z)\epsilon_0\vec{E}$$
$$\vec{\nabla}\times\vec{E}=-j\omega\mu_0\vec{H} \tag{1}$$

we may obtain the vector wave equation

$$\vec{\nabla}\times\frac{1}{\epsilon(\rho,z)}\vec{\nabla}\times\vec{H}-k_0^2\vec{H}=\vec{0} \tag{2}$$

where $k_0^2=\omega^2\mu_0\epsilon_0$ and $\epsilon(\rho,z)$ describes the relative permittivity in all regions. Note that since the geometry is axisymmetric, the permittivity is azimuthally independent; i.e., it does not depend on ϕ. By using Galerkin's method [13], we obtain the bilinear functional $F(H_\phi^c,H_\phi)$:

$$F(H_\phi^C,H_\phi)=\iint_\Omega\left[\left(\frac{1}{\epsilon(\rho,z)}\vec{\nabla}\times\vec{H}\right)\cdot\left(\vec{\nabla}\times H_\phi^c\hat{\phi}\right)-k_0^2H_\phi^cH_\phi\right]\rho\,d\rho\,dz$$
$$+\sum_{\iota=1}^{2}\int_{\Gamma_\iota}\left[\left(\frac{1}{\epsilon(\rho,z)}\vec{\nabla}\times\vec{H}\right)\times H_\phi^c\hat{\phi}\right]\cdot d\vec{l}=0 \tag{3}$$

where Ω is the cross-sectional area of the region and Γ_ι are the port boundaries. H_ϕ^c is a testing function. Note that because of the azimuthal symmetry of the geometry, the problem may effectively be considered as two-dimensional, as indicated by the limits of integration in the bilinear functional. Care must be taken when evaluating the line integral term so that proper normal vectors are taken for each port boundary surface.

To ensure that the FEM analysis is maintained over a finite domain, we must satisfactorily truncate the finite element mesh. In other words, we must enforce boundary conditions at the input and output ports such that the field behavior is correctly represented at these locations. The boundary integral term in the bilinear functional may be rewritten as

$$\int_{\Gamma_\iota}\left[\left(\frac{1}{\epsilon(\rho,z)}\vec{\nabla}\times\vec{H}\right)\times H_\phi^c\hat{\phi}\right]\cdot d\vec{l}=\int_{\Gamma_\iota}\frac{1}{\epsilon(\rho,z)}\left(\rho H_\phi^c\frac{\partial H_\phi}{\partial z}\hat{z}\right)\cdot d\vec{l}. \tag{4}$$

At the input port Γ_1 at $z=-l_1$, the field is composed of the incident and scattered fields, i.e., $H_\phi=H_\phi^i+H_\phi^s$. The fundamental mode (TEM) is used for the incident field, and the port is located at a distance sufficient for higher order evanescent modes to be neglected. We may extend the approach formulated by Mittra and Ramahi [14] for the so-called absorbing boundary condition, which has primarily been used for the electromagnetic scattering problem. Modifying this approach, we obtain

$$\left.\frac{\partial H_\phi}{\partial z}\right|_{z=-l_1}=jk_1\left(H_\phi-2H_\phi^i\right)|_{z=-l_1} \tag{5}$$

where $H_\phi^i=e^{-jk_1z}/\eta_1\rho$ is the fundamental mode excitation of the magnetic field and ϵ_{r1} and η_1 are, respectively, the relative permittivity and the wave impedance at port 1; $\vec{dl}=-\hat{z}\,d\rho$; and $k_1=k_0\sqrt{\epsilon_{r1}}$. Similarly, at the output port Γ_2 at $z=l_2$, the field is composed of only the transmitted field; the absorbing boundary condition is hence

$$\left.\frac{\partial H_\phi}{\partial z}\right|_{z=l_2}=-jk_2H_\phi|_{z=l_2}. \tag{6}$$

The parameter ϵ_{r2} is the relative permittivity at port 2; $\vec{dl}=\hat{z}\,d\rho$; and $k_2=k_0\sqrt{\epsilon_{r2}}$. As with the input port, the evanescent modes are neglected.

To avoid any problem with singular terms in the evaluation of the bilinear functional $F(H_\phi^c,H_\phi)$ as ρ approaches zero, the substitutions $H_\phi=\sqrt{\rho}\,h_\phi$ and $H_\phi^c=\sqrt{\rho}\,h_\phi^c$ are applied. The problem is now in terms of h_ϕ, which is the quantity that will be approximated. The corresponding bilinear functional $F(h_\phi^c,h_\phi)$ is now

$$F(h_\phi^c,h_\phi)=\int\int_\Omega\left\{\frac{1}{\epsilon(\rho,z)}\left[\frac{9}{4}h_\phi^ch_\phi+\rho^2\frac{\partial h_\phi^c}{\partial\rho}\frac{\partial h_\phi}{\partial\rho}+\rho^2\frac{\partial h_\phi^c}{\partial z}\frac{\partial h_\phi}{\partial z}+\frac{3}{2}\left(\rho h_\phi^c\frac{\partial h_\phi}{\partial\rho}+\rho\frac{\partial h_\phi^c}{\partial\rho}h_\phi\right)\right]-k_0^2\rho^2h_\phi^ch_\phi\right\}d\rho\,dz$$
$$+\frac{jk_0}{\sqrt{\epsilon_{r1}}}\left\{\int_{\Gamma_1}\left[\rho^2h_\phi^ch_\phi-\frac{2e^{-jk_1z}}{\eta_1}\left(\sqrt{\rho}\,h_\phi^c\right)\right]d\rho\right\}\Bigg|_{z=-l_1}$$
$$+\frac{jk_0}{\sqrt{\epsilon_{r2}}}\left\{\int_{\Gamma_2}\rho^2h_\phi^ch_\phi\,d\rho\right\}\Bigg|_{z=l_2}=0. \tag{7}$$

The physical system of arbitrary cross section with inhomogeneous dielectrics may be approximated by locally homogeneous subregions throughout which $\epsilon(\rho,z)$ is constant. Triangular subregions are generally chosen because of their flexibility in modeling complicated boundaries. The choice of the order of approximation varies from problem to problem. The use of few high-order elements may produce better results than a correspondingly larger number of low-order elements. Fig. 2 gives examples of first-order and second-order triangular elements. First-order elements correspond to a linear approximation of the unknown, with three nodes per element. Second-order elements correspond to a quadratic approximation, with six nodes per element [9].

IV. Mode Matching

The mode-matching approach adopted in this paper is very similar to that of [12]. Hence only a brief discussion of the method used to formulate the problem will be presented in this section.

The tangential electric and magnetic field components in each region may be expressed in terms of an orthogonal set of vectors which indicate the direction and transverse behavior for each mode. We hence refer to $\vec{e}_s$ and $\vec{h}_s$ as the modal vectors for the sth mode of the electric and magnetic fields. We may express the fields in each region as follows:

$$\vec{E}_\rho^{\,\mathrm{I}}(\rho,z) = \vec{e}_0^{\,\mathrm{I}} e^{-\gamma_0^{\mathrm{I}} z} + \sum_{s=0}^{\infty} b_s^{\mathrm{I}} \vec{e}_s^{\,\mathrm{I}} e^{\gamma_s^{\mathrm{I}} z} \tag{8}$$

$$\vec{H}_\phi^{\,\mathrm{I}}(\rho,z) = \vec{h}_0^{\,\mathrm{I}} e^{-\gamma_0^{\mathrm{I}} z} - \sum_{s=0}^{\infty} b_s^{\mathrm{I}} \vec{h}_s^{\,\mathrm{I}} e^{\gamma_s^{\mathrm{I}} z} \tag{9}$$

$$\vec{E}_\rho^{\,\mathrm{II}}(\rho,z) = \sum_{s=0}^{\infty} \left[a_s^{\mathrm{II}} e^{-\gamma_s^{\mathrm{II}} z} + b_s^{\mathrm{II}} e^{\gamma_s^{\mathrm{II}}(z-d)} \right] \vec{e}_s^{\,\mathrm{II}} \tag{10}$$

$$\vec{H}_\phi^{\,\mathrm{II}}(\rho,z) = \sum_{s=0}^{\infty} \left[a_s^{\mathrm{II}} e^{-\gamma_s^{\mathrm{II}} z} - b_s^{\mathrm{II}} e^{\gamma_s^{\mathrm{II}}(z-d)} \right] \vec{h}_s^{\,\mathrm{II}} \tag{11}$$

$$\vec{E}_\rho^{\,\mathrm{III}}(\rho,z) = \sum_{s=0}^{\infty} a_s^{\mathrm{III}} \vec{e}_s^{\,\mathrm{III}} e^{-\gamma_s^{\mathrm{III}}(z-d)} \tag{12}$$

$$\vec{H}_\phi^{\,\mathrm{III}}(\rho,z) = \sum_{s=0}^{\infty} a_s^{\mathrm{III}} \vec{h}_s^{\,\mathrm{III}} e^{-\gamma_s^{\mathrm{III}}(z-d)} \tag{13}$$

where γ_s is the wavenumber for the sth mode. The modal coefficients a_s and b_s correspond to, respectively, the forward- and backward-traveling modes in each region.

Enforcing the condition of tangential field continuity at the interfaces of regions I and II ($z=0$) and regions II and III ($z=d$) (see Fig. 1), henceforth known as apertures A and B respectively, we obtain

$$\vec{E}_\rho^{\,\mathrm{I}}(\rho,0) = \vec{e}_0^{\,\mathrm{I}} + \sum_{s=0}^{\infty} b_s^{\mathrm{I}} \vec{e}_s^{\,\mathrm{I}} = \vec{E}_\rho^{\,\mathrm{II}}(\rho,0) = \sum_{s=0}^{\infty} \left[a_s^{\mathrm{II}} + b_s^{\mathrm{II}} e^{-\gamma_s^{\mathrm{II}} d} \right] \vec{e}_s^{\,\mathrm{II}} = \vec{E}_{\rho_A} \tag{14}$$

$$\vec{H}_\phi^{\,\mathrm{I}}(\rho,0) = \vec{h}_0^{\,\mathrm{I}} - \sum_{s=0}^{\infty} b_s^{\mathrm{I}} \vec{h}_s^{\,\mathrm{I}} = \vec{H}_\phi^{\,\mathrm{II}}(\rho,0) = \sum_{s=0}^{\infty} \left[a_s^{\mathrm{II}} - b_s^{\mathrm{II}} e^{-\gamma_s^{\mathrm{II}} d} \right] \vec{h}_s^{\,\mathrm{II}} \tag{15}$$

$$\vec{E}_\rho^{\,\mathrm{II}}(\rho,d) = \sum_{s=0}^{\infty} \left[a_s^{\mathrm{II}} e^{-\gamma_s^{\mathrm{II}} d} + b_s^{\mathrm{II}} \right] \vec{e}_s^{\,\mathrm{II}} = \vec{E}_\rho^{\,\mathrm{III}}(\rho,d) = \sum_{s=0}^{\infty} a_s^{\mathrm{III}} \vec{e}_s^{\,\mathrm{III}} = \vec{E}_{\rho_B} \tag{16}$$

$$\vec{H}_\phi^{\,\mathrm{II}}(\rho,d) = \sum_{s=0}^{\infty} \left[a_s^{\mathrm{II}} e^{-\gamma_s^{\mathrm{II}} d} - b_s^{\mathrm{II}} \right] \vec{h}_s^{\,\mathrm{II}} = \vec{H}_\phi^{\,\mathrm{III}}(\rho,d) = \sum_{s=0}^{\infty} a_s^{\mathrm{III}} \vec{h}_s^{\,\mathrm{III}} \tag{17}$$

where $\vec{E}_{\rho A}$ and $\vec{E}_{\rho B}$ are the aperture electric fields.

Defining an energy product

$$\langle \vec{f}, \vec{g} \rangle = \iint_{\mathrm{APERTURE}} \left(\vec{f} \times \vec{g} \right) \cdot d\vec{S} \tag{18}$$

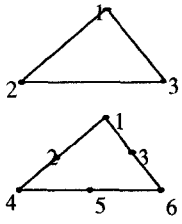

Fig. 2. Triangular mesh elements for finite element modeling.

we may use orthogonality relations to obtain expressions for the modal coefficients in terms of the aperture electric fields and modal vectors. Taking the energy product with the tangential electric field continuity expression (eqs. (14) and (16)) using the corresponding magnetic modal vectors for each region produces explicit expressions for b_s^{I}, a_s^{II}, b_s^{II}, and a_s^{III}. Substituting these expressions into the magnetic field continuity expressions (eqs. (15) and (17)) and rearranging, we obtain

$$\vec{\Lambda}_{AA} + \vec{\Lambda}_{AB} = \vec{h}_0^{\,\mathrm{I}} \tag{19}$$

$$\vec{\Lambda}_{BA} + \vec{\Lambda}_{BB} = \vec{0} \tag{20}$$

where

$$\vec{\Lambda}_{AA} = \sum_{s=0}^{\infty} \frac{\langle \vec{E}_{\rho_A}, \vec{h}_s^{\,\mathrm{I}} \rangle}{\langle \vec{e}_s^{\,\mathrm{I}}, \vec{h}_s^{\,\mathrm{I}} \rangle} \vec{h}_s^{\,\mathrm{I}} + \sum_{s=0}^{\infty} \left(\frac{1+e^{-2\gamma_s^{\mathrm{II}} d}}{1-e^{-2\gamma_s^{\mathrm{II}} d}} \right) \frac{\langle \vec{E}_{\rho_A}, \vec{h}_s^{\,\mathrm{II}} \rangle}{\langle \vec{e}_s^{\,\mathrm{II}}, \vec{h}_s^{\,\mathrm{II}} \rangle} \vec{h}_s^{\,\mathrm{II}} \tag{21}$$

$$\vec{\Lambda}_{AB} = -2 \sum_{s=0}^{\infty} \left(\frac{e_s^{-2\gamma \mathrm{II} d}}{1-e^{-2\gamma_s^{\mathrm{II}} d}} \right) \frac{\langle \vec{E}_{\rho_B}, \vec{h}_s^{\,\mathrm{II}} \rangle}{\langle \vec{e}_s^{\,\mathrm{II}}, \vec{h}_s^{\,\mathrm{II}} \rangle} \vec{h}_s^{\,\mathrm{II}} \tag{22}$$

$$\vec{\Lambda}_{BA} = -2 \sum_{s=0}^{\infty} \left(\frac{e^{-2\gamma_s^{\mathrm{II}} d}}{1-e^{-2\gamma_s^{\mathrm{II}} d}} \right) \frac{\langle \vec{E}_{\rho_A}, \vec{h}_s^{\,\mathrm{II}} \rangle}{\langle \vec{e}_s^{\,\mathrm{II}}, \vec{h}_s^{\,\mathrm{II}} \rangle} \vec{h}_s^{\,\mathrm{II}} \tag{23}$$

$$\vec{\Lambda}_{BB} = \sum_{s=0}^{\infty} \left(\frac{1+e^{-2\gamma_s^{\mathrm{II}} d}}{1-e^{-2\gamma_s^{\mathrm{II}} d}} \right) \frac{\langle \vec{E}_{\rho_B}, \vec{h}_s^{\,\mathrm{II}} \rangle}{\langle \vec{e}_s^{\,\mathrm{II}}, \vec{h}_s^{\,\mathrm{II}} \rangle} \vec{h}_s^{\,\mathrm{II}} + \sum_{s=0}^{\infty} \frac{\langle \vec{E}_{\rho_B}, \vec{h}_s^{\,\mathrm{III}} \rangle}{\langle \vec{e}_s^{\,\mathrm{III}}, \vec{h}_s^{\,\mathrm{III}} \rangle} \vec{h}_s^{\,\mathrm{III}}. \tag{24}$$

Since the energy product is an integral, we now have a system of integral equations for the unknowns $\vec{E}_{\rho A}$ and $\vec{E}_{\rho B}$, which may be solved using a standard moment method technique [15].

V. Numerical Results

Figs. 3 and 4 show geometries, similar to that which may be found in high-frequency connectors, for which the above two methods were applied. Both configurations were excited by an incident TEM field. The reflection and transmission coefficients were computed along with the aperture electric field distributions at both the input and output ports for a frequency of 4 GHz and a separation distance of $d=2$ mm. The dielectric is Teflon, with

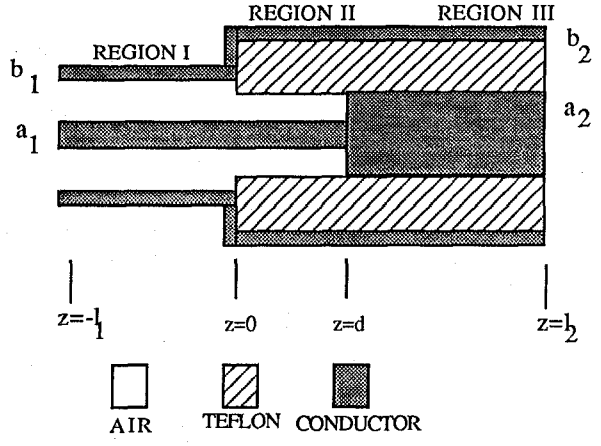

Fig. 3. Cross-sectional view of coaxial line containing step discontinuities.

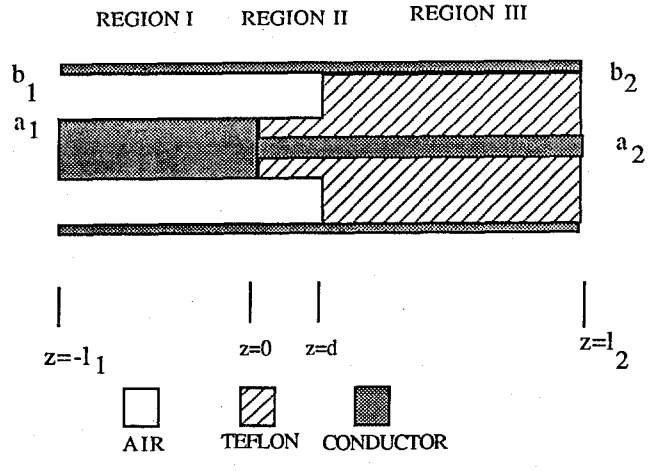

Fig. 4. Modified coaxial geometry with step discontinuities.

relative permittivity $\epsilon_r = 2.03$. For all cases the ratios of the outer to inner conductor radii are $b_1/a_1 = 2.30$ and $b_2/a_2 = 3.28$. This corresponds to a characteristic impedance of 50 Ω for the respective homogeneous regions. Figs. 5 and 6 are FEM results showing the variation of the magnitude and phase of the aperture electric fields versus the radial coordinate for the original geometry (Fig. 3). First- and second-order triangular elements were used for Figs. 5 and 6, respectively. Note that the second-order results are obtained with significantly fewer triangular elements (1011) than required by first-order results (3415). In both cases there is an electric field discontinuity at aperture A, which is consistent with the natural boundary conditions. The transmission and reflection coefficients are also indicated. Fig. 7 is a comparison of the magnitude of the reflection coefficient using both FEM and mode-matching techniques. Figs. 8 and 9 illustrate similar results for the modified geometry (Fig. 4). Fig. 8 shows second-order FEM results, and Fig. 9, a comparison of FEM and mode-matching results. For the modified geometry, the field discontinuity is now present at aperture B.

Fig. 10 shows the variation of the magnitude of the reflection coefficient of the modified geometry versus

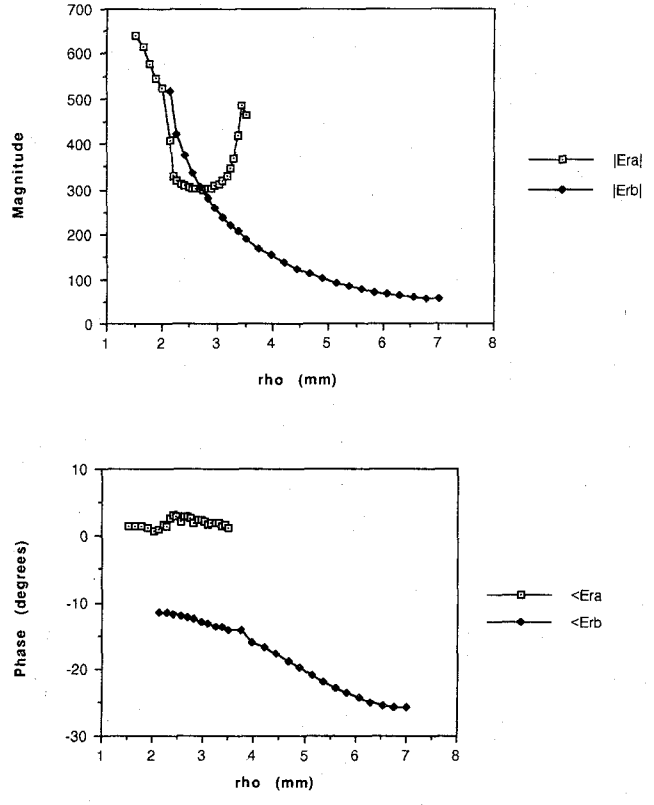

Fig. 5. Aperture electric field distribution for geometry shown in Fig. 3 for $d = 2$ mm using first-order elements (3415 elements). $\Gamma = 0.043\angle -53.81°$. $T = 0.999\angle -14.63°$.

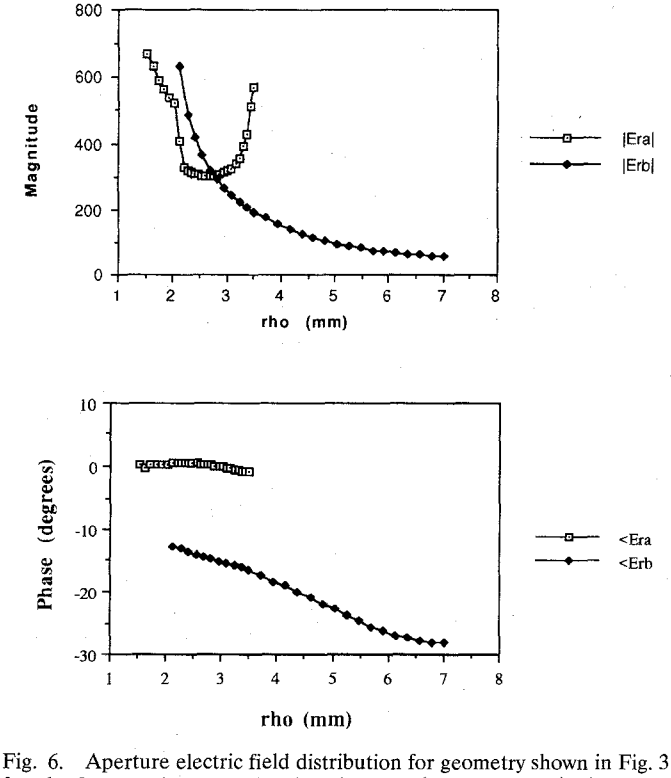

Fig. 6. Aperture electric field distribution for geometry shown in Fig. 3 for $d = 2$ mm using second-order elements (1011 elements). $\Gamma = 0.012\angle -3.331°$. $T = 0.999\angle -17.34°$.

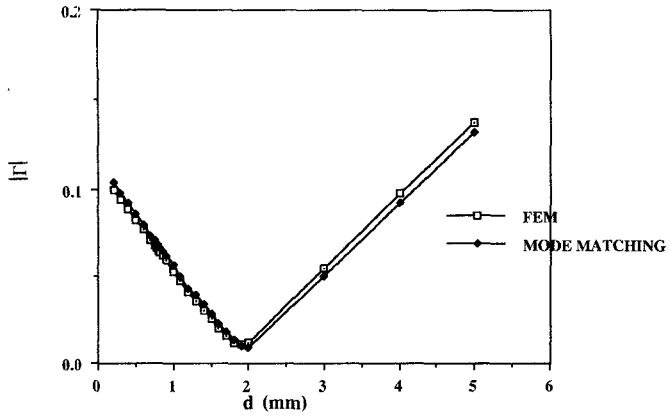

Fig. 7. Comparison of magnitude of reflection coefficient versus discontinuity spacing d as determined using FEM and mode matching (original geometry).

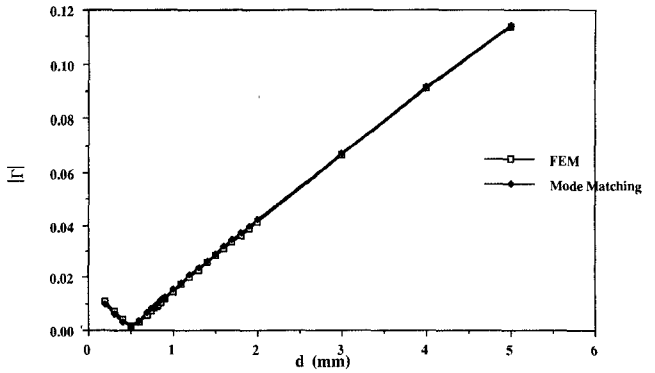

Fig. 9. Comparison of magnitude of reflection coefficient versus discontinuity spacing d as determined using FEM and mode matching (modified geometry).

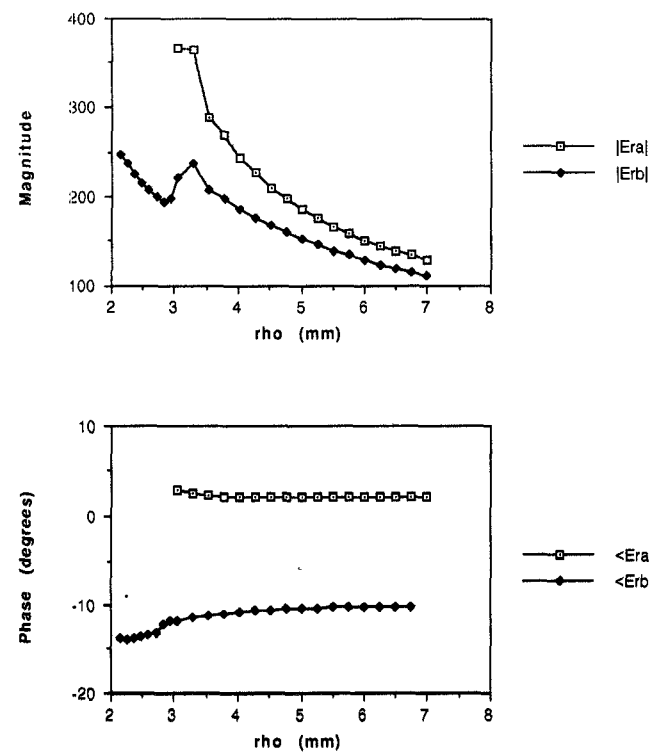

Fig. 8. Aperture electric field distribution for geometry shown in Fig. 4 for $d = 2$ mm using second-order elements (760 elements). $\Gamma = 0.042 \angle -75.43°$. $T = 0.999 \angle -11.27°$.

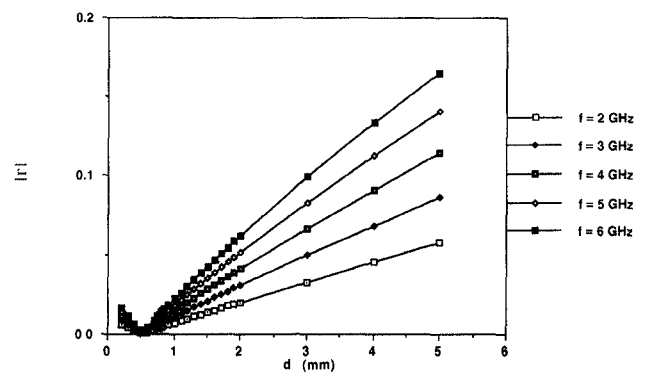

Fig. 10. Variation of magnitude of reflection coefficient versus discontinuity spacing d for modified geometry (various frequencies).

discontinuity spacing d for several frequencies. A point of interest is that the location of minimum reflection in the connectors is independent of frequency. This is a topic for further investigation.

VI. Conclusions and Discussions

The research conducted thus far has been strictly for the cases of lossless materials. This is by no means the limitation of the formulation. These methods, particularly FEM, may be extended to situations where either the dielectrics, the conductors, or both are lossy. We are also not limited by the number of materials which may exist within a given configuration, and owing to the flexibility of FEM, we may look toward solving problems with highly irregular axisymmetric geometries which might otherwise not be feasible by conventional methods. Furthermore, we need not restrict the research to single-mode propagation since, with modifications to the absorbing boundary condition, complete and accurate solutions may be obtained for situations with multimode propagation. All of the aforementioned are topics under current consideration and are hereby proposed for future research.

Acknowledgment

The authors would like to thank Dr. M. I. Aksun, Dr. S. P. Castillo, Dr. C. H. Chan, and Dr. Z. Pantic-Tanner for their helpful technical discussions.

References

[1] N. Marcuvitz, *Waveguide Handbook*. New York: McGraw-Hill, 1951.

[2] J. P. Webb and S. Parihar, "Finite element analysis of H-plane rectangular waveguide problems," *Proc. Inst. Elec. Eng.*, vol. 133, pt. H, pp. 91–94, Apr. 1986.

[3] J. F. Lee and Z. J. Cendes, "An adaptive spectral response modeling procedure for multi-port microwave circuits," *IEEE Trans. Microwave Theory Tech.*, vol. MTT-35, pp. 1240–247, Dec. 1987.
[4] M. Koshiba and M. Suzuki, "Application of the boundary-element method to waveguide discontinuities," *IEEE Trans. Microwave Theory Tech.*, vol. MTT-35, pp. 1240–1247, Dec. 1987.
[5] J. P. Webb, "Absorbing boundary conditions for the finite-element analysis of planar devices," *IEEE Trans. Microwave Theory Tech.*, vol. 38, pp. 1328–1332, Sept. 1990.
[6] A. Konrad, "High-order triangular finite elements for electromagnetic waves in anisotropic media," *IEEE Trans. Microwave Theory Tech.*, vol. MTT-25, pp. 353–360 May 1977.
[7] P. Daly, "An alternative high-order finite element formulation for cylindrical field problems," *Int. J. Numer. Meth. Eng.*, vol. 19, pp. 1063–1072, 1983.
[8] W. K. Gwarek, "Computer-aided analysis of arbitrarily shaped coaxial discontinuities," *IEEE Trans. Microwave Theory Tech.*, vol. 36, pp. 337–342, Feb. 1988.
[9] P. P. Silvester and R. L. Ferrari, *Finite Elements for Electrical Engineers*. Cambridge: Cambridge University Press, 1983.
[10] R. E. Collin, *Field theory of Guided Waves*. New York: McGraw-Hill, 1960.
[11] R. Mittra and S. W. Lee, *Analytical Methods in the Theory of Guided Waves*. New York: Macmillan, 1971.
[12] A. D. Hunt, "Advanced computational characterization of closely coupled coaxial junctions," master's thesis, University of South Florida, Aug. 1989.
[13] G. Strang and G. J. Fix, *An Analysis of the Finite-Element Method*. Englewood Cliffs, NJ: Prentice-Hall, 1973.
[14] R. Mittra and O. Ramahi, "Absorbing boundary conditions for the direct solution of partial differential equations arising in electromagnetic scattering problems," *Differential Methods in Electromagnetic Scattering*, J. A. Kong and M. A. Morgan, Eds. New York: Elsevier, 1989, ch. 4, pp. 133–173.
[15] R. F. Harrington, *Field Computation by Moment Methods*. Malabar, FL: Robert E. Krieger, 1968.

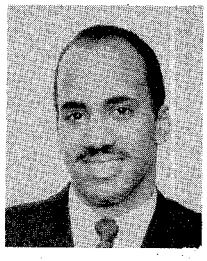

Gregory M. Wilkins (S'90) was born in Washington, DC, on March 3, 1960. He received the degree of bachelor of science in electrical engineering from the University of Maryland, College Park, in 1983 and the master of science degree in electrical engineering from the Johns Hopkins University in 1984. Since 1985 he has been working toward the Ph.D. degree in the Electromagnetic Communication Laboratory at the University of Illinois at Urbana–Champaign. His current research work includes electromagnetic modeling of high-speed digital circuits and electronic packaging.

Mr. Wilkins is a member of Tau Beta Pi, Eta Kappa Nu, the National Society of Black Engineers, and the American Society for Engineering Education.

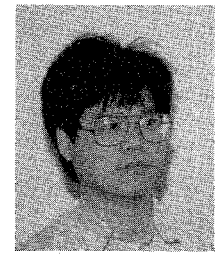

Jin-Fa Lee (S'85–M'88) was born in Taipei, Taiwan, in 1960. He received the B.S. degree from National Taiwan University, Taiwan, in 1982 and the M.S. and Ph.D. degrees from Carnegie Mellon University in 1986 and 1989, respectively, all in electrical engineering.

From 1988 to 1990, he was with the ANSOFT Corporation, where he developed several CAD/CAE finite element programs for modeling three-dimensional microwave and millimeter-wave circuits. In 1990, he left the company to pursue an academic career. Currently, he is a postdoctoral fellow at the Electromagnetic Communication Laboratory, University of Illinois at Urbana–Champaign. His research interests deal with the development of numerical methods for electromagnetic field computation. Current projects include the extension of the FDTD method to nonuniform and unstructured grids, the development of local radiation boundary conditions for three-dimensional electromagnetic scattering, and the application of finite element methods to the modeling of optical fibers.

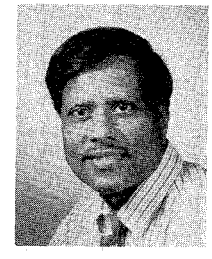

Raj Mittra (S'54–M'57–SM'69–F'71) is the Director of the Electromagnetic Communication Laboratory of the Electrical and Computer Engineering Department and Research Professor of the Coordinated Science Laboratory at the University of Illinois. He is a former president of the IEEE Antennas and Propagation Society and he has served as the editor of the TRANSACTIONS of that society. He won the Guggenheim Fellowship Award in 1965 and the IEEE Centennial Medal in 1984. Currently, he serves as the North American editor of the journal *AEU*. He is President of RM Associates, a consulting organization providing services to several industrial and governmental organizations.

His professional interests include the areas of computational electromagnetics, high-speed digital circuits, radar scattering, satellite antennas, microwave and millimeter-wave integrated circuits, frequency selective surfaces, EMP and EMC analysis, and remote sensing.